Article

Variable-Temperature X-ray Crystallographic and DFT Computational Study of the NH···O/N···HO Tautomeric Competition in 1-(Arylazo)-2-naphthols. Outline of a Transiton-State Hydrogen-Bond Theory

Paola Gilli, Valerio Bertolasi, Loretta Pretto, Liudmil Antonov, and Gastone Gilli

J. Am. Chem. Soc., **2005**, 127 (13), 4943-4953• DOI: 10.1021/ja0453984 • Publication Date (Web): 11 March 2005

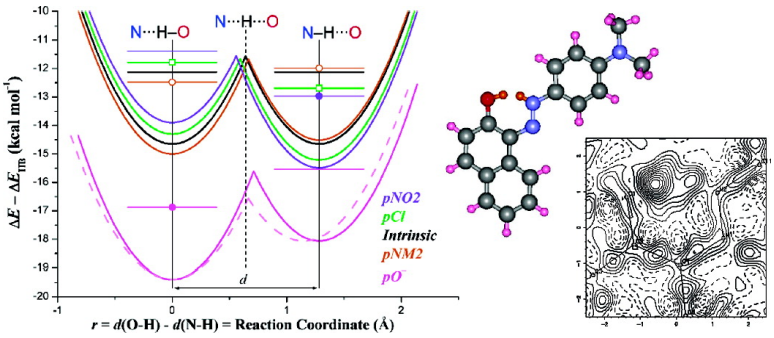

More About This Article

Additional resources and features associated with this article are available within the HTML version:

- Supporting Information
- Links to the 9 articles that cite this article, as of the time of this article download
- Access to high resolution figures
- Links to articles and content related to this article
- Copyright permission to reproduce figures and/or text from this article

View the Full Text HTML

J|A|C|S
ARTICLES
Published on Web 03/11/2005

Variable-Temperature X-ray Crystallographic and DFT Computational Study of the N—H···O/N···H—O Tautomeric Competition in 1-(Arylazo)-2-naphthols. Outline of a Transiton-State Hydrogen-Bond Theory

Paola Gilli,[†] Valerio Bertolasi,[†] Loretta Pretto,[†] Liudmil Antonov,[‡] and Gastone Gilli*,[†]

Contribution from the Centro di Strutturistica Diffrattometrica and Dipartimento di Chimica, Università di Ferrara, I-44100 Ferrara, Italy, and Faculty of Ecology, National Forestry University, Sofia 1756, Bulgaria

Received July 30, 2004; E-mail: ggilli.chim@unife.it

Abstract: Phenyl-substituted 1-arylazo-2-naphthols (AAN) display ···HN—N=C—C=O··· ⇌ ···N=N—C=C—OH··· ketohydrazone−azoenol tautomerism and can form intramolecular resonance-assisted H-bonds from pure N—H···O to pure N···H—O through tautomeric and dynamically disordered N—H···O ⇌ N···H—O bonds according to the electronic properties of their substituents. Three compounds of this series (*m*-OCH_3-AAN = ***mOM***; *p*-Cl-AAN = ***pCl***; and *p*-*N*Me_2-AAN = ***pNM2***) have been studied by X-ray crystallography at four temperatures (100−295 K), showing that the remarkably short H-bonds formed ($2.53 \le d(N\cdots O) \le 2.55$ Å) are a pure N—H···O in ***mOM***, a dynamically disordered mixture in ***pCl*** (N—H···O:N···H—O = 69:31 at 100 K), and a statically disordered mixture in ***pNM2*** (N—H···O:N···H—O = 21:79 at 100 K). These compounds, integrated by the *p*-H-, *p*-NO_2-, *p*-F-, and *p*-O^--substituted derivatives, have been emulated by DFT methods (B3LYP/6-31+G(d,p) level) with full geometry optimization of the stationary points along the proton-transfer (PT) pathway: N—H···O and N···H—O ground states and N···H···O transition state. Analysis of DFT-calculated energies and geometries by the methods of the rate-equilibrium Marcus theory shows that all H-bond features (stability and tautomerism, as well as position and height of the PT barrier) can be coherently interpreted in the frame of the transition-state (or activated-complex) theory by considering the bond as a chemical reaction N—H···O ⇌ N···H···O ⇌ N···H—O which is bimolecular in both directions and proceeds via the N···H···O PT transition state (the activated complex).

Introduction

The resonance-assisted hydrogen-bond (RAHB) model was originally proposed in 1989[1a,b] to account for the abnormally strong intramolecular O—H···O bonds occurring in β-diketone enols (or β-enolones) **I**. From an empirical point of view, it is unambiguosly identified by the strict intercorrelation between hydrogen bond (H-bond) strength (as measured by the O···O distance,[1c,d] the IR ν(O—H) stretching frequency[1e], or the ^{1}H NMR δ(O—H) chemical shift[1f]) and the π-delocalization of the short conjugated chain connecting the H-bond donor and acceptor atoms (as measured by the antisymmetric coordinate $Q = d_1 - d_2 + d_3 - d_4$ or by the π-delocalization index $\langle\lambda\rangle = [(n_1 - 1) + (2 - n_2) + (n_3 - 1) + (2 - n_4)]/4$, where Q = 0.320, 0, −0.320 Å and $\langle\lambda\rangle$ = 0, 0.5, 1 for the enolketo **Ia**, fully π-delocalized **Ic**, and ketoenol **Ib** forms, respectively, and the n_i are Pauling's bond numbers[2] of the bonds d_i).

RAHB has been interpreted as a synergism of H-bond strengthening and enhanced π-delocalization by the use of a number of bonding models.[1a,d,g,3,4] The simplest one, summarized in Scheme 1, is based on the concept of valence bond (VB) resonance between ketoenol and enolketo canonical forms **Ia** ↔ **Ib**,[1d] whose increasing mixing gives rise to different shapes of the proton-transfer (PT) profile which changes from *asymmetric single-well* (**aSW**; **Ie**) to tautomeric *symmetric double-well* (**sDW**; **Id,d′**) to *symmetric single-well* (**sSW**; **Ic**) respectively for moderately strong, strong, and very strong RAHBs.[1g]

[†] Università di Ferrara.
[‡] National Forestry University.

(1) (a) Gilli, G.; Bellucci, F.; Ferretti, V.; Bertolasi, V. *J. Am. Chem. Soc.* **1989**, *111*, 1023. (b) Bertolasi, V.; Gilli, P.; Ferretti, V.; Gilli, G. *J. Am. Chem. Soc.* **1991**, *113*, 4917. (c) Gilli, G.; Bertolasi, V.; Ferretti, V.; Gilli, P. *Acta Crystallogr.* **1993**, *B49*, 564. (d) Gilli, P.; Bertolasi, V.; Ferretti, V.; Gilli, G. *J. Am. Chem. Soc.* **1994**, *116*, 909. (e) Bertolasi, V.; Gilli, P.; Ferretti, V.; Gilli, G. *Chem. Eur. J.* **1996**, *2*, 925. (f) Bertolasi, V.; Gilli, P.; Ferretti, V.; Gilli, G. *J. Chem. Soc., Perkin Trans. 2* **1997**, 945. (g) Gilli, P.; Bertolasi, V.; Pretto, L.; Ferretti, V.; Gilli, G. *J. Am. Chem. Soc.* **2004**, *126*, 3845.

(2) Pauling, L. *J. Am. Chem. Soc.* **1947**, *69*, 542.

(3) (a) Dannenberg, J. J.; Rios, R. *J. Phys. Chem.* **1994**, *98*, 6714. (b) Dannenberg, J. J.; Haskamp, L.; Masunov, A. *J. Phys. Chem. A* **1999**, *103*, 7083. (c) Kobko, N.; Dannenberg, J. J. *J. Phys. Chem. A* **2003**, *107*, 10389. (d) Madsen, G. K. H.; Iversen, B. B.; Larsen, F. K.; Kapon, M.; Reisner, G. M.; Herbstein, F. H. *J. Am. Chem. Soc.* **1998**, *120*, 10040. (e) Schiøtt, B.; Iversen, B. B.; Madsen, G. H. K.; Bruice, T. C. *J. Am. Chem. Soc.* **1998**, *120*, 12117. (f) Grabowski, S. J. *J. Phys. Chem. A* **2001**, *105*, 10739. (g) Grabowski, S. J.; Dubis, A. T.; Martynowski, D.; Glowka, M.; Palusiak, M.; Leszczynski, J. *J. Chem. Phys. A* **2004**, *108*, 5815. (h) Haddon, R. C. *J. Am. Chem. Soc.* **1980**, *102*, 1807. (i) Gatti, C.; Cargnoni, F.; Bertini, L. *J. Comput. Chem.* **2003**, *24*, 422. (j) Munn, R. W.; Eckhardt, C. J. *J. Phys. Chem. A* **2001**, *105*, 6938. (k) Pantano, S.; Alber, F.; Carloni, P. *J. Mol. Struct. (THEOCHEM)* **2000**, *530*, 177.

(4) (a) Gilli, P.; Bertolasi, V.; Ferretti, V.; Gilli, G. *J. Am. Chem. Soc.* **2000**, *122*, 10405. (b) Gilli, P.; Bertolasi, V.; Pretto, L.; Lycka, A.; Gilli, G. *J. Am. Chem. Soc.* **2002**, *124*, 13554. (c) Gilli, G.; Gilli, P. *J. Mol. Struct.* **2000**, *552*, 1.

Scheme 1

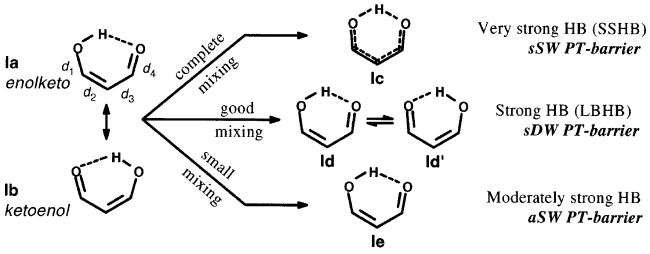

To cope with the most recent H-bond nomenclature,[5] it must be added that the acronyms SSHB (*short-strong H-bond*) and LBHB *(low-barrier H-bond*) are often used to indicate these very strong (**Ic**) and strong and tautomeric (**Id,d′**) H-bonds, respectively.

A further interpretation of RAHB, which will be shown to be particularly useful for the aims of the present paper, relies on what can be called the *PA/pK_a equalization rule*, a simple idea originally proposed in the early 1970s and generally accepted by now,[6] for which H-bond strength is essentially determined, besides the absolute electronegativities of the H-bond donor and acceptor atoms, by the differences of their proton affinities (ΔPA, in the gas phase) or acid−base dissociation constants (ΔpK_a, in liquids and solids), the H-bond being stronger when this difference is smaller. By this rule, it is easy to realize that RAHB strengthens the H-bond because the increasing π-delocalization of the interleaving heterodiene levels out the PA/pK_a difference between the terminal heteroatoms until, in particular conditions, they may become identical (as in **Ic**).[1g,4b] The sum of these two rules, "synergism of H-bond strengthening and enhanced π-delocalization" and "PA/pK_a equalization rule", can be taken as a kind of summary of the empirical rules governing RAHB and should therefore enable us to interpret any case of RAHB occurring in practice.

Starting from this point of view, the essential differences between X−H···X homonuclear and X−H···Y heteronuclear RAHBs can be easily accounted for. In the former, a great ΔPA/ΔpK_a value can be leveled out by complete delocalization of the resonant spacer, while in the latter even such a large delocalization is unable to cope with the intrinsic electronegativity difference of the two heteroatoms, so really strong X−H···Y RAHBs can be achieved only by a proper choice of substituents that are able to further reduce the intrisic PA/pK_a difference. Accordingly, while the literature is full of examples of β-enolones **I** that are able to form short and very short O−H···O RAHBs endowed with symmetrical double-well (**sDW**) and single-well (**sSW**) PT profiles, respectively,[1g] convincing evidence for N−H···O RAHB has been achieved only recently through an extensive screening of the crystal structures of differently substituted β-enaminones and related heterodienes (**II**−**IV**, Scheme 2),[4] which has led, in particular, to single out

Scheme 2

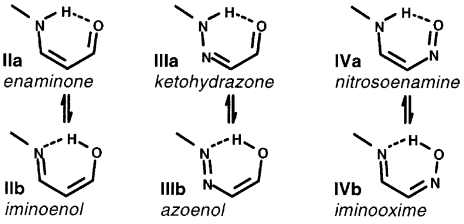

a number of new interesting facts on the role played by aromatic substituents in determining the position of the proton. The case most extensively studied by both X-ray crystallographic and DFT computational methods concerns the N−H···O/N···H−O competition in the ketohydrazone/azoenol system **III**.[4b] Simple ketohydrazones **V** (Scheme 3) inevitably form rather long N−H···O bonds, with N···O distances around 2.67 Å, because the ketohydrazone form **IIIa** is much more stable than its azoenol tautomer **IIIb** in view of the higher PA of nitrogen with respect to oxygen. This second form, however, becomes the more stable one after fusion of the H-bonded ring with a phenylene moiety (**VII**) because the formation of the ketohydrazone tautomer would now require the loss of the large resonance energy of the aromatic ring. Accordingly, the azophenol **VII** is the form normally observed in this class of compounds, with rather short N···O contact distances in the range 2.53−2.61 Å.[7] Fusion with a naphthalene ring, endowed with an intermediate resonance energy value, leads to the more interesting situation of two roughly isoenergetic N−H···O and N···H−O tautomers which can be tuned by the *N*-substituent. Crystal data indicate a large prevalence of rather short N−H···O bonds ($2.50 \le d$(N···O) ≤ 2.55 Å),[4a] though two cases of N···H−O bonds have been also reported for 1-(*p-N,N*-dimethylaminophenylazo)-2-naphthol (d(N···O) = 2.52−2.53 Å)[8a] and 1-(2-thioazolylazo)-2-naphthol (d(N···O) ≃ 2.56 Å).[8b] Quite recently, solid-state N−H···O ⇌ N···H−O dynamic disorder has been shown to occur by variable-temperature X-ray crystallography in 1-(*p*-fluorophenylazo)-2-naphthol and 1-(*o*-fluorophenylazo)-2-naphthol crystals,[4b] where energy differences of only 0.120−0.160 kcal mol^{-1} between the two tautomers have been determined by van't Hoff analysis of H-bond proton populations. Over the years, the problem of the N−H···O/ N···H−O competition in azonaphthols has also prompted a number of studies based on NMR[8a,9a−h] or absorption and fluorescence spectroscopy.[9h−k] NMR solution data have shown that these compounds undergo fast proton exchange on the NMR time scale,[8a,9a−e] while high-resolution ^{15}N and ^{13}C CP/MAS NMR studies indicate equilibrium between N−H···O and N···H−O forms in the solid state, with an energy difference of some 0.4−0.9 kcal mol^{-1} in favor of the former.[8a,9f−h] Finally, in a combined X-ray and NMR study on

(5) (a) Frey, P. A. *Magn. Reson. Chem.* **2001**, *39*, S190. (b) Cleland, W. W. *Biochemistry* **1992**, *31*, 317. (c) Cleland, W. W.; Kreevoy, M. M. *Science* **1994**, *264*, 1887. (d) Frey, P. A.; Whitt, S. A.; Tobin, J. B. *Science* **1994**, *264*, 1927. (e) Cleland, W. W.; Frey, P. A.; Gerlt, J. A. *J. Biol. Chem.* **1998**, *273*, 25529. (f) Harris, T. K.; Mildvan, A. S. *Proteins* **1999**, *35*, 275.

(6) (a) Meot-Ner (Mautner), M. *J. Am. Chem. Soc*. **1984**, *106*, 1257. (b) Meot-Ner (Mautner), M. In *Molecular Structure and Energetics*; Liebman, J. F., Greenberg, A., Eds.; VCH: Weinheim, 1987; Vol. IV, Chapter 3. (c) Zeegers-Huyskens, T. *J. Mol. Struct.* **1986**, *135*, 93. (d) Huyskens, P. L.; Luck, W. A., Zeegers-Huyskens, T., Eds. *Intermolecular Forces*; Springer-Verlag: Berlin, 1991. (e) Malarski, Z.; Rospenk, M.; Sobczyk, L.; Grech, E. *J. Phys. Chem*. **1982**, *86*, 401.

(7) (a) Connor, J. A.; Kennedy, R. J.; Dawes, H. M.; Hursthouse, M. B. *J. Chem. Soc., Perkin Trans. 2* **1990**, 203. (b) Isik, S.; Aygun, M.; Kocaokutgen, H.; Tahir, M. N.; Buyukgungor, O.; Erdonmez, A. *Acta Crystallogr*. **1998**, *C54*, 859. (c) Jimenez-Cruz; F.; Perez-Caballero, G.; Hernandez-Ortega, S.; Rubio-Arroyo, M. *Acta Crystallogr*. **2000**, *C56*, 1028. (d) Pajak, J.; Rospenk, M.; Ramaekers, R.; Maes, G.; Glowiak, T.; Sobczyk, L. *Chem. Phys.* **2002**, *278*, 89. (e) Filarowski, A.; Koll, A.; Glowiak, T.; Majewski, E.; Dziembowska, T. *Ber. Bunsen-Ges. Phys. Chem.* **1998**, *102*, 393. (f) Filarowski, A.; Koll, A.; Glowiak, T. *J. Chem. Soc., Perkin Trans. 2* **2002**, 835. (g) Krygowski, T. M.; Wozniak, K.; Anulewicz, R.; Pawlak, D.; Kolodziejski, W.; Grech, E.; Szady, A. *J. Phys. Chem.* **1997**, *A101*, 9399. (h) Dominiak, P. M.; Grech, E.; Barr, G.; Teat, S.; Mallison, P.; Wozniak, K. *Chem. Eur. J.* **2003**, *9*, 963.

(8) (a) Olivieri, A. C.; Wilson, R. B.; Paul, I. C.; Curtin, D. Y. *J. Am. Chem. Soc.* **1989**, *111*, 5525. (b) Kurahashi, M. *Bull. Chem. Soc. Jpn.* **1976**, *49*, 2927.

Scheme 3

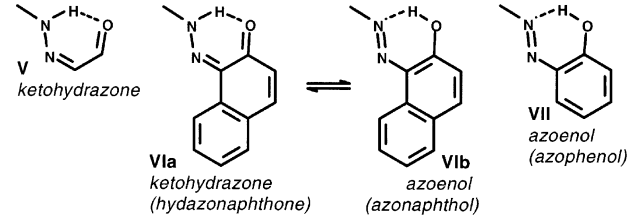

Scheme 4

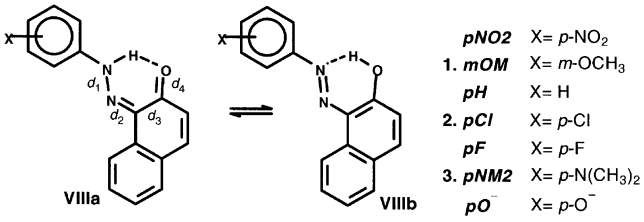

phenyl-substituted 1-arylazo-naphthalen-2-ols **VIII** (Scheme 4), Olivieri et al.[8a] have suggested that electron-withdrawing para-substituents at the *N*-phenyl stabilize the hydrazonaphthalenone form **VIIIa**, while electron-donating ones shift the equilibrium toward the azonaphthol tautomer **VIIIb**, the extreme term tested having been the *p*-dimethylamino derivative, which was found to be disordered with an approximate N—H···O:N···H—O ratio of 1:3, though more precise H-bond proton populations could not be measured.

The present paper is addressed to a more thorough understanding of the effects of phenyl substitution on the features of the N—H···O/N···H—O bond in 1-(arylazo)-2-naphthols (Scheme 4) by two complementary techniques: (i) structure determination of two new arylazonaphthols [**1** = ***mOM*** = 1-(*m*-methoxyphenylazo)-2-naphthol and **2** = ***pCl*** = 1-(*p*-chlorophenylazo)-2-naphthol] and redetermination of 1-(*p*-*N*,*N*-dimethylaminophenylazo)-2-naphthol (**3** = ***pNM2***) by X-ray diffractometry at four different temperatures (100, 150, 200, and 295 K), a technique which has been reported to distinguish between static and dynamic disorder of the H-bond proton,[1g,4b,10] and (ii) DFT quantum-mechanical modeling of the three stationary points (N—H···O, N···H···O (transition-state, TS), and N···H—O) occurring along the PT pathway for the expanded series of seven representative derivatives listed in Scheme 4, followed by correlation of their energetic and geometrical properties by means of the Leffler−Hammond postulate[11a,b] and rate-equilibrium extrathermodynamic Marcus theory,[11c−f] a method already successfully applied to H-bond studies.[4b]

It will be shown that the combined use of these techniques gives a coherent picture of the transition between the N—H···O and N···H—O bonds as a function of the properties of the phenyl substituents, as evaluated from their mesomeric Hammett constants,[12] σ^0_R, a picture which is in substantial agreement with the qualitative predictions originally reported.[8a] It is finally suggested that the correlative methods used here to analyze the simulated PT pathways can be generalized to the treatment of all types of H-bonds other than RAHBs and may constitute a basis for a novel H-bond theory univocally grounded on the results and methods of the transition-state kinetic theory.[11g]

Variable-Temperature X-ray Crystallography

Experimental details are given in the Experimental Section, and complete tables of bond distances and angles in the deposited CIF files (Supporting Information). Table 1 reports a selection of data for **1**−**3** at 100 K, including H-bond geometries, *d*(N···O), *d*(N−H), *d*(O−H), and α(N−H−O), *percent* H-bond proton populations (occupancies), *p*(%), d_1-d_4 bond distances, and π-delocalization parameters $\langle\lambda\rangle$[13] of the resonant N−N−C−C−O fragment. An analogous table for compounds **1**−**3** at the four temperatures investigated (100, 150, 200, and 295 K) is deposited as Table S1 of the Supporting Information. ORTEP[14] views of the molecular structures at 100 K are given in Figures 1a, 2a, and 3a for **1**, **2**, and **3**, respectively. All structures at all temperatures are essentially planar, with the phenyl ring in the plane of the 1-(arylazo)-2-naphthol fragment, the value of the $N_1-N_2-C_{11}-C_{16}$ torsion angle being 4.3(2), −0.4(2), and 3.6(2)° at 100 K for **1**, **2**, and **3**, respectively. Figures 1b, 2b, and 3b display the corresponding difference Fourier maps at 100 K computed in the mean plane of the H-bonded chelated ring after refinement carried out with the exclusion of the H-bonded hydrogen.

Compound 1 (*mOM*). The structure of compound **1** reveals the formation of a rather strong N—H···O bond with N···O distances slightly decreasing from 2.548(2) to 2.541(3) Å on going from 100 to 295 K. The proton position is strongly shifted toward the nitrogen (average *d*(N−H) of 0.98[2] Å against a *d*(H···O) of 1.72[3] Å), as clearly depicted by the difference map of Figure 1b. The H-bond formed can therefore be classified **aSW-HB** (asymmetric single well−high barrier) according to

(9) (a) Lyčka, A. *Dyes Pigm.* **1990**, *12*, 179. (b) Lyčka, A.; Jirman, J.; Nečas, M. *Dyes Pigm.* **1991**, *15*, 23. (c) Hansen, P. E.; Bolvig, S.; Buvari-Barcza, A.; Lyčka, A. *Acta Chem. Scand.* **1997**, *51*, 881. (d) Hansen, P. E.; Sitkowski, J.; Rozwadowski, Z.; Dziembowska, T. *Ber. Bunsen-Ges. Phys. Chem.* **1998**, *102*, 410. (e) Alarcón, S. H.; Olivieri, A. C.; Sanz, D.; Claramunt, R. M.; Elguero, J. *J. Mol. Struct.* **2004**, *705*, 1. (f) Benedict, C.; Langer, U.; Limbach, H.-H.; Ogata, H.; Takeda, S. *Ber. Bunsen-Ges. Phys. Chem.* **1998**, *102*, 335. (g) Takeda, S.; Inabe, T.; Benedict, C.; Langer, U.; Limbach, H.-H. *Ber. Bunsen-Ges. Phys. Chem.* **1998**, *102*, 1358. (h) Alarcón, S. H.; Olivieri, A. C.; Nordon, A.; Harris, R. K. *J. Chem. Soc., Perkin Trans. 2* **1996**, 2293. (i) Joshi, H.; Kamounah, F. S.; van der Zwan, G.; Gooijer, C.; Antonov, L. *J. Chem. Soc., Perkin Trans. 2* **2001**, 2303. (j) Joshi, H.; Kamounah, F. S.; Gooijer, C.; van der Zwan, G.; Antonov, L. *J. Photochem. Photobiol. A* **2002**, *152*, 183. (k) Fabian, W. M. F.; Antonov, L.; Nedeltcheva, D.; Kamounah, F. S.; Taylor, P. J. *J. Phys. Chem. A* **2004**, *108*, 7603.

(10) (a) Destro, R.; Marsh, R. E. *J. Am. Chem. Soc.* **1984**, *106*, 7269. (b) Destro, R. *Chem. Phys. Lett.* **1991**, *118*, 232. (c) Boese, R.; Antipin, M. Yu.; Bläser, D.; Lyssenko, K. A. *J. Phys. Chem. B* **1998**, *102*, 8654. (d) Ogawa, K.; Kasahara, Y.; Ohtani, Y.; Harada, J. *J. Am. Chem. Soc.* **1998**, *120*, 7107. (e) Wilson, C. C. *Acta Crystallogr.* **2001**, *B57*, 435. (f) Wilson, C. C.; Goeta, A. E. *Angew. Chem., Int. Ed.* **2004**, *43*, 2095.

(11) (a) Leffler, J. E. *Science* **1953**, *117*, 340. (b) Hammond, G. S. *J. Am. Chem. Soc.* **1955**, *77*, 334. (c) Marcus, R. A. *Discuss. Faraday Soc.* **1960**, *29*, 21. (d) Marcus, R. A. *J. Phys. Chem.* **1968**, *72*, 891. (e) Shaik, S. S.; Schlegel, H. B.; Wolfe, S. *Theoretical Aspects of Physical Organic Chemistry. The S_N2 Mechanism*; John Wiley: New York, 1992. (f) Grunwald, E. *J. Am. Chem. Soc.* **1985**, *107*, 125. (g) Glasstone, S.; Laidler, K. J.; Eyring, H. *The Theory of Rate Processes*; McGraw-Hill: New York, 1941. (h) Leffler, J. E.; Grunwald, E. *Rates and Equilibria of Organic Reactions*; Wiley: New York, 1963. (i) Thornton, E. R. *J. Am. Chem. Soc.* **1967**, *89*, 2915.

(12) Chapman, N. B., Shorter, J. Eds. *Correlation Analysis in Chemistry*; Plenum Press: New York, 1978; Chapter 10.

(13) Bond numbers, *n*, have been calculated from bond distances, *d*, by the Pauling's formula[2] $d(n) = d(1) - c \log n$, where *d*(*n*) and *d*(1) are the bond lengths for $n = n$ and $n = 1$, respectively, and *c* is a constant to be evaluated for each type of chemical bond. Values for pure single- and double-bond distances [*d*(1) and *d*(2), respectively] used in the calculations are (1.49; 1.33), (1.38; 1.20), (1.41; 1.27) and (1.39; 1.24) Å, respectively, for $C(sp^2)-C(sp^2)$, $C(sp^2)-O$, $C(sp^2)-N(sp^2)$, and $N(sp^2)-N(sp^2)$. The C_1-C_2 bond number was given the reference value of $n = 1.646$ derived from the corresponding $d = 1.375$ Å of the naphthalene structure (Brook, C. P.; Dunitz, J. D. *Acta Crystallogr.* **1982**, *B38*, 2218). $\langle\lambda\rangle$ values are calculated according to the formula given in the Introduction.

(14) Burnett, M. N.; Johnson, C. K. *ORTEP−III: Oak Ridge Thermal Ellipsoids Plot Program for Crystal Structure Illustrations*; Oak Ridge National Laboratory Report ORNL-6895; Oak Ridge National Laboratory: Oak Ridge, TN, 1996.

Table 1. Intramolecular H−Bond Parameters (Å and Deg), Tautomeric H-Bond Proton Occupancies p (%), Selected d_1-d_4 Bond Distances (Å), and π-Delocalization Parameters ($\langle\lambda\rangle$; See Text) of the N−N−C−C−O π-Conjugated Fragment for Compounds **1** (***mOM***), **2** (***pCl***), and **3** (***pNM2***) as Determined by X-ray Diffraction Methods at 100 K (Standard Deviations in Parentheses)

compd	H-bond	N···O	N−H	H−O	N−H−O	p(NH)% p(OH)%	N−N d_1	N−C d_2	C−C d_3	C−O d_4	$\langle\lambda\rangle$
1 (***mOM***)	N−H···O	2.548(2)	1.01[a]	1.71[a]	138[a]	100	1.308(2)	1.337(2)	1.457(2)	1.262(1)	0.45
2 (***pCl***)	N−H···O	2.516(2)	1.01[a]	1.67[a]	139[a]	69(3)	1.308(2)	1.345(2)	1.453(2)	1.276(2)	0.52
	N···H−O		1.70[a]	0.94[a]	143[a]	31(3)					
3 (***pNM2***)	N−H···O	2.534(2)	1.01[a]	1.66[a]	144[a]	21(3)	1.280(1)	1.406(2)	1.402(2)	1.347(1)	0.86
	N···H−O		1.69[a]	0.94[a]	147[a]	79(3)					

[a] N−H and O−H distances have been normalized at 1.01 and 0.94 Å, respectively, and must therefore be considered to have only indicative meaning.

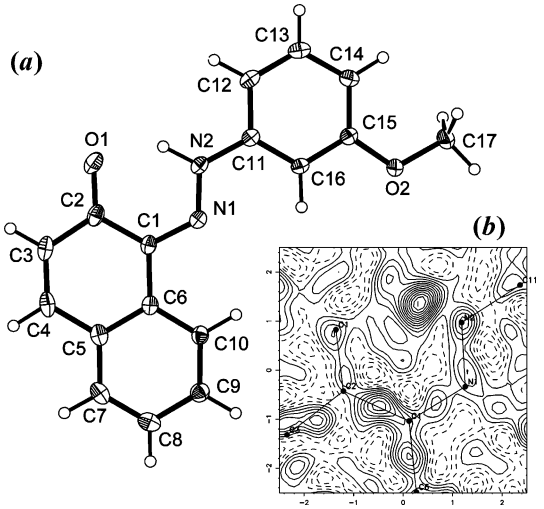

Figure 1. (a) ORTEP[14] view of the molecular structure of compound **1** (***mOM***) as determined at 100 K with thermal ellipsoids at 40% probability. The ordered $N_2-H\cdots O_1$ H-bond is not indicated. (b) Difference Fourier map in the mean plane of the H-bonded ring for compound **1** (***mOM***) at 100 K. The map was computed after least-squares refinement carried out without the H-bond proton. Positive (continuous) and negative (dashed) contours drawn at 0.06 e/Å^3 intervals.

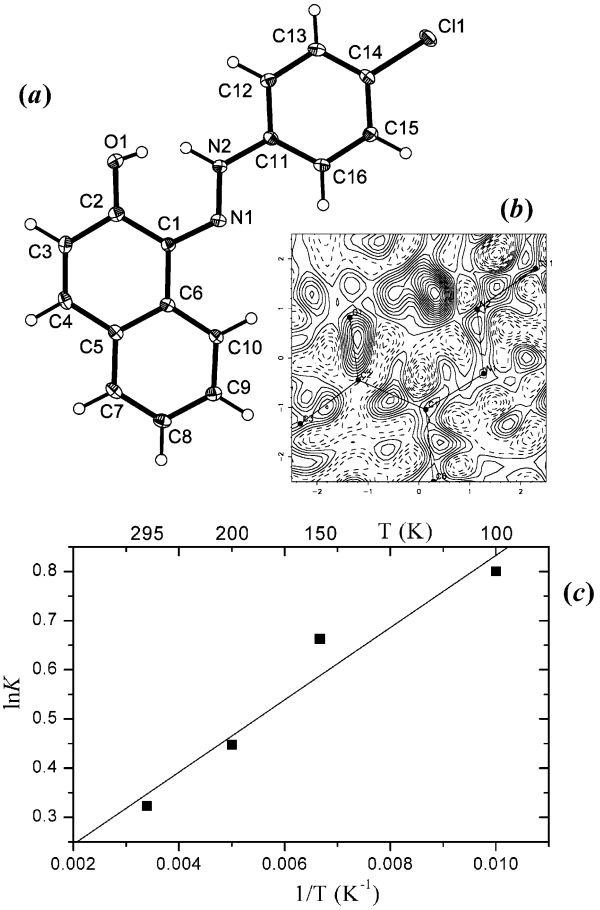

Figure 2. (a) ORTEP[14] view of the molecular structure of compound **2** (***pCl***) as determined at 100 K with thermal ellipsoids at 40% probability. The two tautomeric $N_2-H\cdots O_1$ and $O_1-H\cdots N_2$ H-bonds are not indicated. (b) Difference Fourier map in the mean plane of the H-bonded ring for compound **2** (***pCl***) at 100 K computed as indicated in Figure 1. (c) Van't Hoff plot $\ln K = \Delta S°/R - \Delta H°/R(1/T)$ for compound **2** (***pCl***). $K = p/(1-p)$ is the ratio of the proton populations as derived from least-squares refinement. $\Delta H° = -0.146(25)$ kcal mol^{-1}, $\Delta S° = 0.19(17)$ cal mol^{-1} K^{-1} ($n = 4$, $r = 0.972$).

the nomenclature suggested in ref 1g. The value of $\langle\lambda\rangle = 0.45$ at 100 K shows that the resonant fragment is heavily π-delocalized and could be represented as a 45:55 mixture of the two ···HN−N=C−C=O··· ↔···N=N−C=C−OH··· VB resonant forms.

Compound 2 (*pCl*). The intramolecular H-bond formed is rather stronger than in the previous case, having a N···O distance ranging from 2.516(2) Å at 100 K to 2.520(2) Å at 295 K. Moreover, the H-bond proton is disordered between the N−H···O and N···H−O positions, with proton population ratios ranging with continuity from 69:31 at 100 K to 58:42 at 295 K. The parameters of the tautomeric equilibrium can be determined by van't Hoff linear regression, $\ln K = \Delta S°/R - \Delta H°/R(1/T)$ (Figure 2c), where the equilibrium constant is $K = p(\mathrm{NH})/p(\mathrm{OH}) = p(\mathrm{NH})/(1 - p(\mathrm{NH}))$. Standard enthalpy, $\Delta H°$, and entropy, $\Delta S°$, values of $-0.146(25)$ kcal mol^{-1} and 0.19(17) cal mol^{-1} K^{-1} were obtained. The $\Delta S°$ is not significantly different from zero, as expected for an intramolecular process. The $\Delta H°$ has the meaning of energy difference between the two N−H···O and N···H−O ground-state vibrational levels in a double-minimum potential experienced by the proton. Though the $\Delta H°$ found can only be considered as approximate in view of the uncertainties of the values of crystallographic proton populations, the substantial linearity of the plot seems a clear indication of a fast-exchange equilibrium process of dynamic nature. The H-bond can therefore be classified as a true LBHB[5] of RAHB type with a slightly **aDW-LB** (asymmetric double well−low barrier) PT pathway.[1g] It has been shown previously[4b] that RAHBs which are disordered in the H-bond proton position are also disordered in the resonant fragment, which turns out to be the average of two ···HN−N=C−C=O··· and ···N=N−C=C−OH··· tautomeric groups which simulate an almost complete π-delocalization ($\langle\lambda\rangle = 0.52$ in the present case). This disorder, at variance with that of the proton, is very hard to resolve by diffraction methods but can be easily detected by quantum-mechanical emulation of the geometries of the two tautomers, as illustrated below.

Compound 3 (*pNM2*). The H-bond length is intermediate between those of the two previous compounds, the N···O

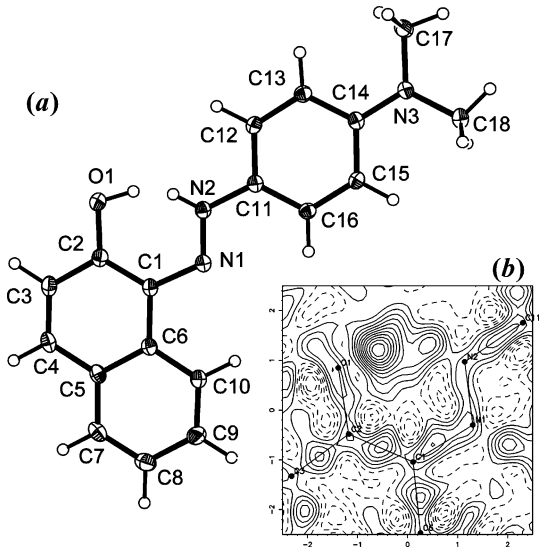

Figure 3. (a) ORTEP[14] view of the molecular structure of compound **3** (***pNM2***) as determined at 100 K with thermal ellipsoids at 40% probability. The two tautomeric $N_2-H\cdots O_1$ and $O_1-H\cdots N_2$ H-bonds are not indicated. (b) Difference Fourier map in the mean plane of the H-bonded ring for compound **3** (***pNM2***) at 100 K computed as indicated in Figure 1.

distance ranging from 2.534(2) Å at 100 K to 2.531(3) Å at 295 K. Also in this case, the proton is disordered over two positions but with a prevalence of the N···H−O tautomer over the N−H···O one. Proton populations are essentially independent of temperature, being, on average, in the ratio 79[1]:21[1]. Data are consistent with a case of static disorder within a slightly **aDW-HB** (asymmetric double well−high barrier) PT profile,[1g] where the delocalization parameter $\langle\lambda\rangle$ (0.86 at 100 K) has the meaning of weighted average of the delocalizations of the two tautomeric forms. The phenyl ring shows an interesting quinoid deformation, the average of the two $C_{12}-C_{13}$ and $C_{15}-C_{16}$ distances (1.378[1] Å with an average Pauling's bond number $n = 1.62$) being significantly shorter than the remaining four phenyl bonds (1.408[8] Å; $n = 1.43$). The fact that the $C_{14}-N_3$ bond is shortened (1.370(2) Å; $n = 1.22$) while the $C_{11}-N_2$ one is not (1.398(2) Å; $n = 1.06$) suggests a definite contribution of the polar form $N_3^+=C_{14}-C=C-C^-_{11}-N_2$, where the partial negative charge is not transmitted beyond the C_{11} atom.

DFT Emulation of H-Bonded Arylazonaphthols

DFT modeling of H-bonded arylazonaphthols has been performed on a series of compounds, including those presently studied by diffraction methods (**1** = ***mOM***, **2** = ***pCl***, and **3** = ***pNM2***), implemented by four other molecules intended to cover the largest range of electron-donating or -withdrawing properties of the phenyl substituents. These new compounds include 1-(*p*-nitrophenylazo)-2-naphthol (***pNO2***), 1-(phenylazo)-2-naphthol (***pH***), 1-(*p*-fluorophenylazo)-2-naphthol (***pF***), and 1-(*p*-hydroxyphenylazo)-2-naphthol anion (***pO***$^-$). Crystal structures for ***pNO2***,[15a] ***pH***,[8a,15b,c] and ***pF***[4b] have been previously reported, and DFT computations for ***pH*** and ***pF*** have ben taken from ref 4b. All calculations were performed by using the Gaussian 98 package[16a] at the B3LYP/6-31+G(d,p)//B3LYP/6-31+G(d,p) level of theory by (i) full geometry optimization of both N−H···O and N···H−O tautomers in the C_s point group; (ii) TS localization by the QST2 method;[16b] and (iii) vibrational analysis for energy zero-point correction (ZPC) and check of the actual planarity of all molecules at their three stationary points.

Final results are summarized in Table 2, while some further geometrical parameters are given in Table S2 of the Supporting Information. ΔE and ΔE_{ZPC} are the noncorrected and ZP-corrected energies of the stationary points relative to the TS chosen as zero. In terms of PT reaction pathway, they assume the meaning of the negative of *energy barriers*, $\Delta^{\ddagger}E$ and $\Delta^{\ddagger}E_{ZPC}$, for the PT process in the two directions, while the energy differences between the two minima, ΔE_r, is that of *reaction energies* which turn out to be fairly similar before and after ZP correction because ZPC has the nearly constant value of 2.52[11] kcal mol^{-1} for all the series investigated. RC = [d(O−H) − d(N−H)] is the *reaction coordinate* for the PT process, while $d = RC_{N-H\cdots O} - RC_{N\cdots H-O}$ is the *total length of the PT pathway*. It is advantageous to rescale RC to the *relative reaction coordinate*, $r = RC - RC_{N\cdots H-O}$ ($0 \le r \le d$), or to the *fractional reaction coordinate*, r/d ($0 \le r/d \le 1$).

While X-ray experimental structures of compounds forming an ordered N−H···O (***pNO2***, ***mOM***, and ***pH***) or N···H−O bond (***pO***$^-$, if its structure were available) can be directly compared with the corresponding N−H···O or N···H−O DFT-computed geometries, structures displaying N−H···O ⇌ N···H−O disorder (***pCl***, ***pF***, and ***pNM2***) can only be compared with the average value of the N−H···O and N···H−O computed ones, weighted according to the X-ray-determined proton populations. By using this method of comparison, the agreement on bond distances turns out to be fairly good, with average and maximum discrepancies of 0.007 and 0.023 Å, respectively, while differences on H-bond N···O distances are in the range 0.004−0.009 Å, with the only exception of ***pCl*** (0.030 Å).

The compounds of Table 2 are arranged in order of increasing values of ΔE_r, which range from −1.59 kcal mol^{-1} for ***pNO2*** to 1.34 kcal mol^{-1} for ***pO***$^-$. While ΔE_r increases, the stable H-bond form is seen to move from pure N−H···O (***pNO2***, ***mOM***, and ***pH***) to two coexisting N−H···O ⇌ N···H−O tautomers (***pCl***, ***pF***, and ***pNM2***) up to pure N···H−O (***pO***$^-$), in substantial agreement with the X-ray findings summarized in the column "X-rays" in Table 2. The TS always corresponds to the shortest possible bond along the pathway (d(N···O) = 2.38−2.40 Å), while the two N−H···O and N···H−O minima are associated with two H-bonds that, besides being rather longer (d(N···O) = 2.53−2.56 Å), differ by an amount, Δ, which changes regularly with ΔE_r, being 0.026 Å for ***pNO2***, decreasing monotonically to nearly zero for ***pF*** and ***pNM2***, and becoming negative (−0.012 Å) for ***pO***$^-$. This phenomenon can be

(15) (a) Whitaker, A. *Z. Kristallogr.* **1980**, *152*, 227. (b) Salmen, R.; Malterud, K. E.; Pedersen, B. F. *Acta Chem. Scand.* **1988**, *A42*, 493. (c) Chongyang, L.; Lynch, V.; Bard, A. J. *Chem. Mater.* **1997**, *9*, 943.

(16) (a) Frisch, M. J.; Trucks, G. W.; Schlegel, H. B.; Scuseria, G. E.; Robb, M. A.; Cheeseman, J. R.; Zakrzewski, V. G.; Montgomery, J. A., Jr.; Stratmann, R. E.; Burant, J. C.; Dapprich, S.; Millam, J. M.; Daniels, A. D.; Kudin, K. N.; Strain, M. C.; Farkas, O.; Tomasi, J.; Barone, V.; Cossi, M.; Cammi, R.; Mennucci, B.; Pomelli, C.; Adamo, C.; Clifford, S.; Ochterski, J.; Petersson, G. A.; Ayala, P. Y.; Cui, Q.; Morokuma, K.; Rega, N.; Salvador, P.; Dannenberg, J. J.; Malick, D. K.; Rabuck, A. D.; Raghavachari, K.; Foresman, J. B.;. Cioslowski, J.; Ortiz, J. V.; Baboul, A. G.; Stefanov, B. B.; Liu, G.; Liashenko, A.; Piskorz, P.; Komaromi, I.; Gomperts, R.; Martin, R. L.; Fox, D. J.; Keith, T.; Al-Laham, M. A.; Peng, C. Y.; Nanayakkara, A.; Challacombe, M.; Gill, P. M. W.; Johnson, B.; Chen, W.; Wong, M. W.; Andres, J. L.; Gonzalez, C.; Head-Gordon, M.; Replogle, E. S.; Pople, J. A. *GAUSSIAN 98*, Revision A.11.3; Gaussian, Inc.: Pittsburgh, PA, 2002. (b) Ayala, P. Y.; Schlegel, H. B. *J. Chem. Phys.* **1997**, *107*, 375.

Table 2. DFT Stationary-Point Energies (kcal mol^{-1}) and Geometries (Å and Deg) along the PT Pathway of the Intramolecular N−H···O/N···H−O Bond in 1-(Phenylazo)-2-naphthols Variously Substituted at the Phenyl Ring[a]

compd	H-bond	$\Delta E = -\Delta^{\ddagger}E$	$\Delta E_{ZPC} = -\Delta^{\ddagger}E_{ZPC}$	N···O	N−H	H−O	N−H−O	RC	r	$r^{\ddagger}/d$	$\langle\lambda\rangle$	ΔE_{HB}	X-rays	σ^0_R
pNO2	N−H···O	−3.83	−1.44	2.555•	1.037	1.699	136.7	0.662	1.287		0.41	15.5•	N−H···O	
	TS	0	0	2.384	1.262	1.201	150.8	−0.061	0.564	0.438	0.60	11.7	**aSW**	0.17
	N···H−O	−2.23	0.12	2.529	1.633	1.008	145.3	−0.625	0		0.74	13.9	ordered	
	ΔE_r	−1.59	−1.56	$\Delta = 0.026$				$d = 1.287$						
mOM	N−H···O	−3.82	−1.32	2.557•	1.037	1.700	136.9	0.663	1.293		0.44	16.3•	N−H···O	
	TS	0	0	2.386	1.256	1.209	150.9	−0.047	0.583	0.451	0.63	12.5	**aSW**	−
	N···H−O	−2.55	−0.05	2.534	1.638	1.008	145.5	−0.630	0		0.78	15.0	ordered	
	ΔE_r	−1.26	−1.27	$\Delta = 0.023$				$d = 1.293$						
pH	N−H···O	−3.69	−0.99	2.555•	1.038	1.695	137.1	0.657	1.289		0.44	15.7•	N−H···O	
	TS	0	0	2.386	1.253	1.211	150.9	−0.042	0.590	0.458	0.63	12.0	**aSW**	0
	N···H−O	−2.58	−0.11	2.535	1.640	1.008	145.4	−0.632	0		0.78	14.6	ordered	
	ΔE_r	−1.11	−0.88	$\Delta = 0.020$				$d = 1.289$						
pCl	N−H···O	−3.64	−0.94	2.550*	1.039	1.688	137.2	0.649	1.285		0.45	15.2*	N−H···O/N···H−O = 69:31	
	TS	0	0	2.384	1.249	1.214	150.9	−0.035	0.601	0.468	0.63	11.6	slightly **aDW**	−0.29
	N···H−O	−2.72	−0.31	2.536*	1.643	1.007	145.3	−0.636	0		0.75	14.3*	dynamically disordered	
	ΔE_r	−0.91	−0.63	$\Delta = 0.014$				$d = 1.285$					(LBHB)	
pF	N−H···O	−3.33	−0.65	2.546*	1.039	1.681	137.5	0.642	1.282		0.44	14.6*	N−H···O/N···H−O = 64:36	
	TS	0	0	2.384	1.246	1.218	150.9	−0.028	0.612	0.477	0.63	11.3	nearly **sDW**	−0.40
	N···H−O	−2.93	−0.36	2.538*	1.646	1.006	145.3	−0.640	0		0.78	14.2*	dynamically disordered	
	ΔE_r	−0.40	−0.29	$\Delta = 0.008$				$d = 1.282$					(LBHB)	
pNM2	N−H···O	−2.65	−0.15	2.541*	1.043	1.663	138.6	0.620	1.261		0.49	14.5*	N−H···O/N···H−O = 21:79	
	TS	0	0	2.388	1.234	1.232	151.0	−0.002	0.639	0.507	0.66	11.9	slightly **aDW**	−0.53
	N···H−O	−3.14	−0.70	2.541*	1.647	1.006	145.6	−0.641	0		0.81	15.0*	statically disordered	
	ΔE_r	0.49	0.55	$\Delta = 0.000$				$d = 1.261$						
pO$^-$	N−H···O	−1.44	0.97	2.527	1.060	1.596	143.3	0.536	1.147		0.60	18.1	N···H−O	
	TS	0	0	2.404	1.225	1.251	147.5	0.026	0.637	0.555	0.69	16.6	**aSW**	−0.60
	N···H−O	−2.78	−0.30	2.539•	1.625	1.014	152.3	−0.611	0		0.76	19.4•	ordered (predicted)	
	ΔE_r	1.34	1.28	$\Delta = -0.012$				$d = 1.147$						

[a] ΔE and ΔE_{ZPC} = noncorrected and zero-point-corrected (ZPC) stationary-point energies relative to the TS chosen as zero; Δ = difference between the N···O distances of the N−H···O and N···H−O bonds; RC = [d(O−H) − d(N−H)] = reaction coordinate; $d = RC_{N-H\cdots O} - RC_{N\cdots H-O}$ = total reaction pathway length; $r = RC - RC_{N\cdots H-O}$ = relative RC; $r^{\ddagger}/d$ = TS fractional RC; $\langle\lambda\rangle = \pi$-delocalization parameter (see text) of the N−N−C−C−O π-conjugated fragment; ΔE_{HB} = H−bond energy computed comparing the open and closed (H-bonded) N···H−O forms; X-rays = comparison between DFT and X-ray determined structures; **SW**, **DW** = single-, double-well; **a**, **s** = asymmetric, symmetric; σ^0_R = mesomeric constant of the para substituent.[12] In columns N···O and ΔE_{HB}, the unique stable form is indicated by a full point and the tautomeric pairs by asterisks.

interpreted[4b] in terms of the Leffler−Hammond postulate,[11a,b] stating that the closer a minimum is to the TS position, the more it participates in its geometrical structure. Since the H-bond at the TS is always the shortest, in a tautomeric couple such as N−H···O ⇌ N···H−O the H-bond closer to the TS (the less stable one) is shorter than that which is farther (the more stable one), a difference which will fade when the PT barrier becomes symmetrical ($\Delta E_r = 0$). This symmetry can also be appreciated through the value of the fractional reaction coordinate at the TS, $r^{\ddagger}/d$, which is ≃0.5 for ***pF*** and ***pNM2***, while it is out-centered for the other compounds with extremes of 0.438 and 0.555 for ***pNO2*** and ***pO***$^-$, respectively.

Bond distances, d_1-d_4, and π-delocalization parameters, $\langle\lambda\rangle$ (Tables 2 and S2, and Scheme 4), of the N−N−C−C−O resonant fragment make it possible to interpret more precisely the phenomena of disorder often observed in the X-ray structures of these compounds. In the crystal structure of **1** (***mOM***), the proton is involved in an ordered N−H···O bond and, accordingly, the resonant moiety assumes a geometry shifted toward the ketohydrazo form **VIa** with a $\langle\lambda\rangle_{EXP}$ of 0.45 (Table 1), a value which is well reproduced by the DFT-emulated molecule in its N−H···O form ($\langle\lambda\rangle_{CALC} = 0.44$). Conversely, the proton is disordered in compound **2** (***pCl***) in the ratio N−H···O:N···H−O = 69:31 at 100 K with an apparent $\langle\lambda\rangle_{EXP}$ of 0.52, which in itself has no precise meaning because also the resonant fragment must be a 69:31 mixture of ketohydrazo and azoenol tautomers of unknown $\langle\lambda\rangle$. Table 2 gives now calculated values of 0.45 and 0.75 for such individual tautomers, allowing us to estimate $\langle\lambda\rangle_{CALC} = 0.69(0.45) + 0.31(0.75) = 0.54$, which compares well with the experimental value. Similar calculations can be performed for ***pNM2*** (**3**) ($\langle\lambda\rangle_{CALC} = 0.21(0.49) + 0.79(0.81) = 0.74$ against $\langle\lambda\rangle_{EXP} = 0.86$ at 100 K) and ***pF***[4b] ($\langle\lambda\rangle_{CALC} = 0.64(0.44) + 0.36(0.78) = 0.56$ against $\langle\lambda\rangle_{EXP} = 0.55$ at 100 K) and contribute to making it clear that the disorder in the RAHB proton necessarily implies a similar disorder in the resonant fragment and that, if this has not been experimentally detected, it can only be because of the insufficient resolution of the present X-ray diffraction experiments.

Finally, Table 2 reports the estimated H-bond energies, ΔE_{HB}, of the three stationary points calculated starting from the N···H−O form, whose ΔE_{HB} is easily computed by comparing the energies of the closed (H-bonded) and open forms of the molecule, the latter being obtained by 180° rotation of the proton around the C−OH bond (values reported do not take into account ZPC; corrected ones, $\Delta E_{HB,ZPC}$(N···H−O), are smaller by only 0.3−0.7 kcal mol^{-1}). The ΔE_{HB} of the more stable tautomer remains nearly constant (some 15.4 kcal mol^{-1}) from ***pNO2*** to ***pNM2***, where the N−H···O bond is prevalent or, at least, one of the two possible forms, but steeply increases to 19.4 kcal mol^{-1} for the N···H−O bond in ***pO***$^-$, for which some shortening of the total length of the PT pathway is also found ($d = 1.147$ Å against an average value of 1.283 Å), suggesting

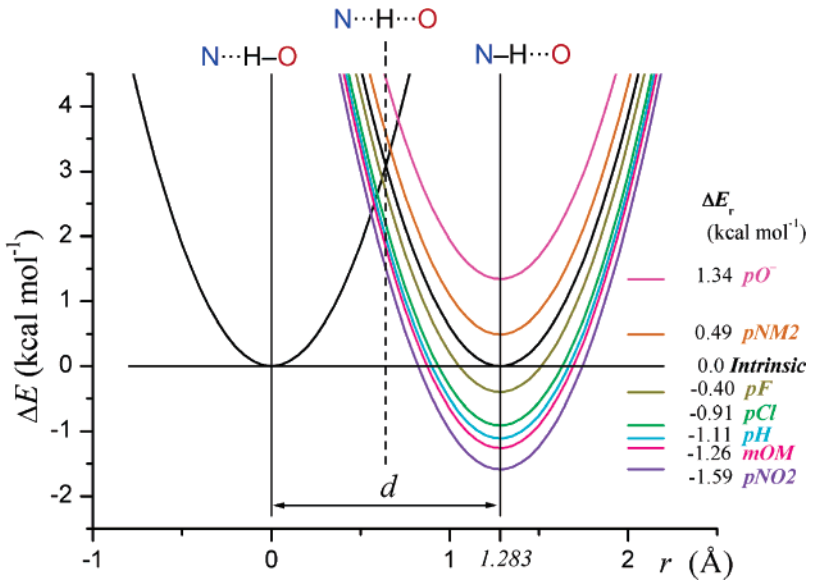

Figure 4. Marcus modeling[11c−f] of the N···H−O → N−H···O PT reaction by the use of DFT-calculated data not corrected for ZPC (force constant, k = 15.0 kcal mol^{-1} Å^{-2}; total PT transfer pathway length, d = 1.283 Å). The two symmetric parabolas (in black) cross at the intrinsic barrier value $\Delta^{\ddagger}E_o$ = 3.08 kcal mol^{-1} for $r^{\ddagger}/d$ = 0.5. Curves for the other compounds (in color) are shifted upward or downward by their respective reaction energies, ΔE_r, and cross at $r^{\ddagger}/d$ values larger or smaller than 0.5 and PT barriers $\Delta^{\ddagger}E$ higher or lower than $\Delta^{\ddagger}E_o$, respectively.

that the N···H−O bond is intrinsically stronger than the N−H···O one in this class of compounds. In agreement with the general criterion that H-bond energies steeply decrease when the bond becomes less linear,[17] the greater stability of the N···H−O bond can be accounted for by the different equilibrium values of the N−N−H and C−O−H angles (some 116 and 106°, respectively), which make the N−H−O angle much less bent in the N···H−O case (152.3° in ***pO***$^-$) than in the N−H···O one (on average, 137° from ***pNO2*** to ***pF***). Since such a ΔE_{HB} difference seems to be basically due to the steric constraints imposed by the intramolecular H-bonded ring closure, it may be supposed that it will not be observed in strain-free intermolecular H-bonds.

Marcus Analysis of DFT Data

The interrelationships among the different parameters characterizing the PT reaction pathway can be established in the frame of the rate-equilibrium extrathermodynamic Marcus theory[11c−f] which represents, for the specific H-bond case, the reactant (N···H−O) and the product (N−H···O) of the PT process N···H−O → N−H···O as simple harmonic oscillators with the same force constant k but shifted by d, and having respective energies E(N···H−O) = $^1/_2kr^2$ and E(N−H···O) = $\Delta E_r + {}^1/_2k(r - d)^2$ (see Figure 4). These two curves cross at the TS position ($r = r^{\ddagger}$) at an energy value which represents, with respect to the minima of the two parabolas, the energy barriers, $\Delta^{\ddagger}E$, for the direct and reverse PT processes. The particular barrier, $\Delta^{\ddagger}E_o$, occurring for ΔE_r = 0, i.e., when the H-bond donor and acceptor atoms have identical PA (or identical pK_a), is called the *intrinsic barrier* (see the two intercrossing black curves of Figure 4). The H-bond occurring in connection with such an intrinsic barrier is called the *intrinsic H-bond*[4b] and corresponds to the 1:1 population ratio of the two tautomers separated by the lowest possible barrier in the DW system considered. Mathematical relationships[11c−f] among variables are summarized by the three equations:

$$\Delta^{\ddagger}E = \Delta^{\ddagger}E_o + \Delta E_r/2 + (\Delta E_r)^2/(16\Delta^{\ddagger}E_o) \quad (1)$$

$$r^{\ddagger}/d = \Delta E_r/(kd^2) + 1/2 \quad (2)$$

$$k = 8\Delta^{\ddagger}E_o/d^2 \quad (3)$$

For each specific ΔE_r of Table 2, eq 1 allows us to calculate, by a simple recursive technique, the corresponding value of $\Delta^{\ddagger}E_o$, while eq 2 gives us that of the vibrational force constant k. These two sets of values were then averaged to obtain $\Delta^{\ddagger}E_o$ = 3.08 kcal mol^{-1} and k = 15.0 kcal mol^{-1} Å^{-2}, two values which can be shown to be perfectly consistent through eq 3. The agreement between Marcus- and DFT-calculated values (Table S3 and Figures S1 and S2 of the Supporting Information) is generally fairly good, with the exception of the $\Delta^{\ddagger}E$ values of ***pO***$^-$, which are calculated some 1.0 kcal mol^{-1} too high (see below). The results of the Marcus modeling are graphically summarized in Figure 4, where the two parabolas at the same height (ΔE_r = 0) and shifted by d (in black) cross at the intrinsic (symmetric) barrier value of 3.08 kcal mol^{-1} for $r^{\ddagger}/d$ = 0.5, while the other curves (in color), which represent the actual compounds studied, are shifted upward or downward by their respective ΔE_r values and cross at $r^{\ddagger}$ values larger or smaller than $d/2$ with $\Delta^{\ddagger}E$ values higher or lower than $\Delta^{\ddagger}E_o$, respectively, in agreement with the Leffler−Hammond rule.[11a,b]

The application of a Marcus-type treatment (eqs 1−3) to the DFT stationary-point energies and geometries is quite able, therefore, to reduce all compounds of Table 2 to a single coherent reaction series having a common intrinsic barrier and whose chemical properties are continuously modulated by substitutions outside the formal reaction zone.[11f,h,i] One must be careful, however, not to force wrong physical interpretations of Figure 4, where the two intersecting curves are representative of the Marcus formalism applied but do not have the meaning originally associated with it. Normal Marcus parabolas and corresponding activation energies represent pure diabatic VB

(17) (a) Lippincott, E. R.; Schroeder, R. *J. Chem. Phys.* **1955**, *23*, 1099. (b) Schroeder, R.; Lippincott, E. R. *J. Phys. Chem.* **1957**, *61*, 921.

states, which are in fact mathematical constructs. They will represent the actual adiabatic PT pathway only after correction for the mixing of these VB diabatic states which, while producing only a small stabilization of the N—H···O and N···H—O ground states, may induce a large lowering of the PT barrier[18] which is greater for stronger H-bonds (see the state-correlation diagram for O—H···O RAHB in ref 1g). Because of the holistic nature of MO calculations, mixing corrections are already accounted for in our calculated ground and TS energy values, and, accordingly, the Marcus curves of Figures 4 and 5 describe the true adiabatic PT pathways, whose parametric values ($\Delta^{\ddagger}E_o$ and k) should now have the actual physical meaning for the reaction series studied.[19]

The energy barriers so far discussed neglect the zero vibrational level of the proton, which has been shown above to be some 2.52 kcal mol^{-1}, giving a first estimate of the intrinsic barrier corrected for ZP vibrations as $\Delta^{\ddagger}E_{o,ZPC} = 3.08-2.52 = 0.56$ kcal mol^{-1}. A reasonably similar result ($\Delta^{\ddagger}E_{o,ZPC} = 0.46$ kcal mol^{-1}) is obtained by applying eq 1 to the $\Delta^{\ddagger}E_{ZPC}$ values of Table 2 (see Table S3), and a value of 0.495 kcal mol^{-1} has been reported in a previous paper[4b] for another series of ketohydrazones/azoenols containing also two arylazonaphthols. There is little doubt, therefore, that the $\Delta^{\ddagger}E_{o,\ ZPC}$ is in the range 0.46−0.56 kcal mol^{-1}. Rather, the real problem that remains is how, precisely, DFT calculations can reproduce the true values of the PT barriers, a point often discussed but for which no simple answer has been given so far.[20]

Finally, the combined information arising from Marcus analysis and DFT-computed ΔE_{HB} values is summarized in Figure 5, which should represent the total energy of the system with respect to a zero, different for any of the different molecules, representing their energy in a hypothetical non-H-bonded (open) state. The black curve corresponds to the intrinsic H-bond, whose ΔE_{HB} was evaluated as an average of ***pF*** and ***pNM2***, the two compounds approaching, from opposite sides, the condition $\Delta E_r = 0$. Some compounds (***mOM***, ***pH***, and ***pF***) have been omitted to avoid overcrowding in the N—H···O region, and also because they do not add much to the general picture. For compound ***pO***$^-$, two different curves are reported, representing the outcome of the Marcus modeling (continuous) and the exact curve derivable from the actual DFT parameters of Table 2 (dashed). Though the differences are significant, they are certainly not such to endanger the general conclusions drawn from the Marcus analysis. Figure 5 also reports the approximate vibrational levels of the proton, estimated to have the constant value of 2.52 kcal mol^{-1} (see above). In agreement with expectation, in compounds forming pure N—H···O (***pNO2***) or N···H—O bonds (***pO***$^-$), the vibrational levels of the unstable forms are higher than the PT barrier, while in the two tautomeric compounds (***pCl*** and ***pNM2***) both of these levels lie slightly below it.[21] This seems an indication that the values of DFT-calculated barriers cannot be very far from the real ones.

Discussion

X-ray diffraction as well as solid-state and solution NMR experiments agree in indicating that phenyl-substituted aryl-azonaphthols may be a quite interesting series of compounds in view of their ability to form intramolecular H-bonds which are switchable from pure N—H···O to pure N···H—O through tautomeric N—H···O ⇌ N···H—O bonds by modeling the electron-withdrawing or -donating properties of the phenyl substituent. In this paper we have attempted to rationalize the different experimental findings by an analysis of the energies and geometries of a congruous series of these compounds, as emulated through quantum-mechanical DFT calculations. The method, already discussed in a previous paper,[4b] is a simple extension of the well-known transition-state (or activated-complex) theory[11g] to H-bond studies, according to which any X—H···Y bond can be considered as a chemical reaction X—H···Y ⇌ X···H···Y ⇌ X···H—Y which is bimolecular in both directions and proceeds via the X···H···Y PT trasition state (the activated complex). The essential difference with respect to normal chemical reactions is that both reactants and products are pre-bound by the H-bond, so that rather small PT barriers

(18) (a) Warshel, A.; Hwang, J. K.; Åqvist, J. *Faraday Discuss.* **1992**, *93*, 225. (b) Hwang, J. K.; King, G.; Creighton, S.; Warshel, A. *J. Am. Chem. Soc.* **1988**, *110*, 5297. (c) Schutz, C. N.; Warshel, A. *J. Phys. Chem. B* **2004**, *108*, 2066. (d) Warshel, A. *Computer Modeling of Chemical Reactions in Enzymes and Solutions*; John Wiley and Sons: New York, 1991. (e) Hwang, J. K.; Warshel, A. *J. Am. Chem. Soc.* **1996**, *118*, 11745. (f) Warshel, A.; Weiss, R. M. *J. Am. Chem. Soc.* **1980**, *102*, 6218. (g) Åqvist, J.; Warshel, A. *Chem. Rev.* **1993**, *93*, 2523.

(19) Though the application of eqs 1−3 to the present DFT data may appear straightforward, it is important to point out some underlying problems of interpretation that can be fully appreciated only in the framework of the modified Marcus theory of Warshel and co-workers by making use of the Hwang−Åqvist−Warshel (HAW) expression[18a−c] for the calculation of the reaction activation barrier, $\Delta^{\ddagger}g$. According to the symbols used in eq 1, such an equation can be written as

$$\Delta^{\ddagger}g = w^r + (\Delta E_r + \lambda)^2/4\lambda - \bar{H}_{12}(r^{\ddagger}) + \bar{H}_{12}(r_o)^2/(\Delta E_r + \lambda) - \Gamma$$

where (i) the first term, w^r, is the work to bring the reactants to their reacting configuration (in the present case equal to zero); (ii) the second is formally identical to the Marcus eq 1 rewritten for $\lambda = 4(\Delta^{\ddagger}E_o)_{dia}$; (iii) the third, $\bar{H}_{12}(r^{\ddagger})$, is the lowering of the diabatic crossing, $(\Delta^{\ddagger}E_o)_{dia}$, of the Marcus parabolas at $r^{\ddagger}$ due to resonance mixing between the reactants and the products; (iv) the fourth is the analogous but usually much smaller lowering of the ground state at $r_o = 0$ or $r_o = d$; and finally, (v) the last term is a correction that reflects tunneling effects (not considered here) and ZP vibrational corrections for light atoms such as hydrogens (accounted for in our calculations). In the Warshel's empirical valence bond (EVB) method,[18d−g] the different terms of eq 4 are separately evaluated, in particular $(\Delta^{\ddagger}E_o)_{dia}$, the Marcus diabatic intrinsic PT barrier, and $\bar{H}_{12}(r^{\ddagger})$, which is (by neglecting the smaller perturbation of the ground state) the correction needed to calculate the lower adiabatic one. When, however, calculations are performed by MO methods (either ab initio or DFT), things change because the calculated energies of the three stationary points already include $\bar{H}_{12}(r^{\ddagger})$ and $\bar{H}_{12}(r_o)$ for transition and ground states, respectively, so that, always neglecting the small lowering of the ground state, the $\Delta^{\ddagger}E_o$ of eq 1 can only represent the *true adiabatic PT barrier*, that is, $\Delta^{\ddagger}E_o(\text{eq 1}) = (\Delta^{\ddagger}E_o)_{adia} = (\Delta^{\ddagger}E_o)_{dia} - \bar{H}_{12}(r^{\ddagger})$. It is interesting but not really surprising[11f] that, even after this correction, data still fit a Marcus-type equation, as shown by Figure 4 and Table S3, but with the substantial differences that the PT barrier is now physically more meaningful (i.e., adiabatic) because it is already corrected for $\bar{H}_{12}$, and that the vibrational constant, k, is now the smaller but more realistic anharmonic one instead of the larger and harmonic constant which is typical of the Marcus formalism. For similar reasons, Marcus-type pathways of Figures 4 and 5 do now intersect the correct energy values of the three stationary points, though their slopes cannot be considered to depict the exact shape of the PT pathways (fully optimized DFT-emulated ground-state pathways for compounds ***pH*** and ***pF***, obtained by QST3 method,[16b] have been reported in Figure 5 of ref 4b). These considerations, which account well for the low values of both intrinsic barrier and vibrational constants found in the present work, seem to make it clear that the meaning of the Marcus analysis is not the same in VB and MO applications, but that these differences can be understood and rationalized by the use of the more comprehensive treatment based on the HAW equation.[18a−c]

(20) (a) Koch, W.; Holthausen, M. C. *A Chemist's Guide to Density Functional Theory*, 2nd ed.; Wiley-VCH: Weinheim, 2001. (b) Barone, V.; Adamo, C. *J. Chem. Phys.* **1996**, *105*, 11007.

(21) It is rather surprising that ***pNM2***, having an even smaller PT barrier than the dynamically disordered compound ***pCl*** (Table 2), displays static instead of dynamic proton disorder within a nearly 200 K temperature range. This anomaly seems to suggest a larger coupling constant among N—H···O ⇌ N···H—O PT reaction centers within the crystal of ***pNM2*** with respect to ***pCl***, which can be due to the spreading of the ***pNM2*** reaction center through the quinoid π-delocalization of the *p*-dimethylaminophenyl group, as well as to specific features of the packing arrangement. It may be significant that multinuclear NMR studies of ***pNM2*** in a variety of organic solvents indicate[9e] a dynamical equilibrium of N—H···O and N···H—O forms with ratios ranging from 19:81 to 28:72, in strict agreement with our crystallographic ratio of 21:79.

are to be expected. Analysis of DFT data is performed by the Marcus rate-equilibrium extrathermodynamic relationships (eqs 1−3),[11c−f] whose application to the present system has been described in some detail above, resulting in a number of interesting observations which deserve to be summarized in a more concise and rational form:

(a) DFT data can be consistently fitted using a value of force constant $k = 15.0$ kcal mol^{-1} Å^{-2} = 0.027 mdyn Å^{-1} = 0.027 N cm^{-1}, corresponding to some 75 cm^{-1} as evaluated by the DFT vibrational analysis of these compounds. This force constant is some 250 times smaller than those associated with normal N−H or O−H bonds (6−8 N cm^{-1})[22] and can only be ascribed to the NH···O or N···HO stretching vibration of the H-bond itself, in agreement with early far-infrared measurements which consistently suggested values of 80−250 cm^{-1}.[23]

(b) The properties of the N−H···O ⇌ N···H−O equilibrium can be fully described in terms of these two wide nonbonded vibrations, shifted by $d = 1.283$ Å (Figure 4) and intercrossing with an intrinsic PT barrier $\Delta^{\ddagger}E_o = 3.08$ kcal mol^{-1}, which is reduced to $\Delta^{\ddagger}E_{o,ZPC} = 0.46-0.56$ kcal mol^{-1} by taking into account ZP correction.

(c) This intrinsic barrier is low enough to allow H-bond dynamical disorder (LBHB) for ΔE_r values close to zero, and pure N−H···O or N···H−O bonds for $\Delta E_r \lesssim -1.0$ or $\Delta E_r \gtrsim 1.0$ kcal mol^{-1}, respectively.

(d) The DFT-calculated values of ΔE_r predict almost perfectly the type of H-bond (N−H···O, N−H···O ⇌ N···H−O, N···H−O) actually found in the corresponding crystal structures (column "X-ray" of Table 2).

(e) The shortest N···O distance is always associated with the TS stationary point (2.38−2.40 Å) whose energy is, however, greater than that of the thermodynamically stable H-bonds. This makes clear why the present N−H···O/N···H−O RAHB system cannot form the very short and strong **SW** H-bonds (SSHBs) typical of some O···H···O RAHBs but only, at its maximum, strong LBHBs when $\Delta E_r \simeq 0$ (cf. Scheme 1). In fact, such very short **SW** SSHBs must have the structure of a TS with negative intrinsic PT barrier ($\Delta^{\ddagger}E_o < 0$),[1g] an event impossible for arylazonaphthols, whose lowest barrier still amounts to 0.46−0.56 kcal mol^{-1}.

In conclusion, the properties of any X−H···Y H-bonded system are univocally determined by only two fixed parameters ($\Delta^{\ddagger}E_o$ and k, or $\Delta^{\ddagger}E_o$ and d), while ΔE_r is the only independent variable which represents the thermodynamic driving force of the system having the plausible physical meaning of ΔPA, the proton affinity difference between the H-bond donor and acceptor atoms. This quantity cannot be either measured or calculated for intramolecular RAHBs but can be tentatively related to the extrathermodynamic LFER parameters of the phenyl para or meta substituents.[12] In the present case, ΔE_r does not correlate with the usual para and meta Hammett constants (σ_p and σ_m) but rather with the mesomeric constant, σ^0_R, which can seem logical in view of the resonance-assisted nature of the H-bond formed. The ΔE_r versus σ^0_R plot is shown in Figure 6 for all the compounds of Table 2 except ***mOM***, for which σ^0_R has no precise meaning. Since both σ^0_R and ΔE_r have

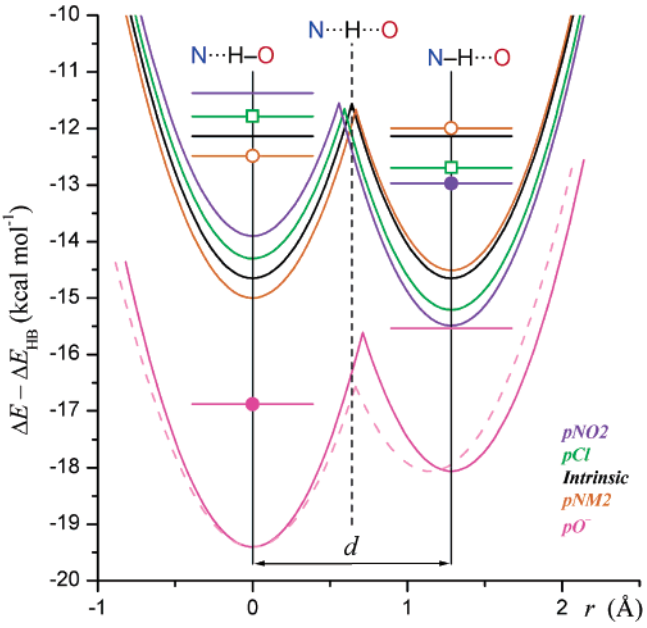

Figure 5. Combined information arising from the Marcus modeling and the DFT-computed H-bond energies, ΔE_{HB}, of Table 2 for a selection of the compounds treated in Figure 4. The black curve corresponds to the *intrinsic H-bond* having $\Delta E_r = 0$ and $\Delta^{\ddagger}E = \Delta^{\ddagger}E_o$. Horizontal lines mark the approximate vibrational levels of the proton; full points indicate single-well and open symbols double-well H-bonds. The dashed curve is an alternative treatment of the ***pO***$^-$ DFT data (see text).

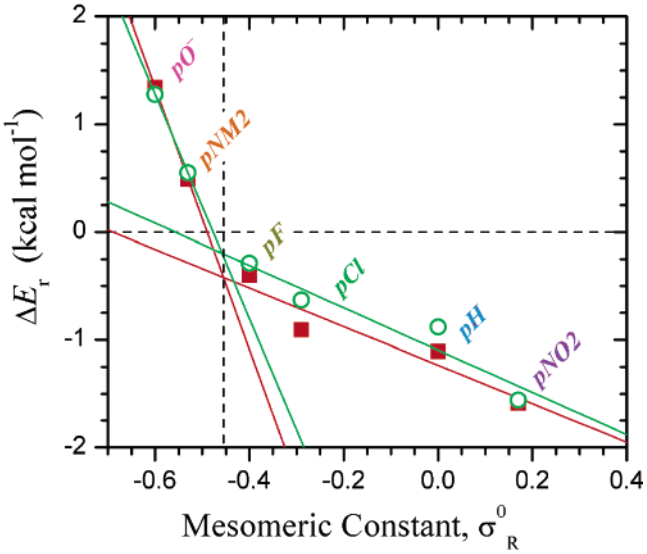

Figure 6. Plot of the DFT-calculated reaction energies, ΔE_r, as a function of the mesomeric constant σ^0_R of the phenyl para substituent.[12] Following Leffler and Grunwald,[24] the two straight lines indicate that the two N−H···O → N···H−O and N···H−O → N−H···O reactions have different PT mechanisms. Red and green lines and symbols refer to uncorrected and ZPC-corrected DFT-calculated data.

dimensions of an energy, the plot could be expected to consist of a unique straight line and not, as actually found, of two intercrossing lines with rather different slopes. According to Leffler and Grunwald,[24] this change of slope is characteristic of chemical reactions which change their mechanism of action beyond a certain value of σ^0_R, suggesting again that the two N−H···O → N···H−O and N···H−O → N−H···O reactions may have different features in the intramolecular system

(22) *CRC Handbook of Chemistry and Physics*, 75th ed.; Lide, D. R., Frederikse, H. P. R., Eds.; CRC Press: Boca Raton, FL, 1994; pp 9−74.
(23) Vinogradov, S. N.; Linnel, R. H. *Hydrogen Bonding*; Van Nostrand Reinhold: New York, 1971; pp 71−74.
(24) Chapter 7 of ref 11h.

considered in conjunction with the intuitive idea that electronic effects of the substituents are felt much more strongly by N than by O in this class of molecules and with the sudden change of H-bond energetic and geometric properties associated with the transition from N—H···O to N···H—O (Figure 5 and end of discussion of Table 2).

Experimental Section

Variable-Temperature Crystal Structure Analysis. X-ray diffraction data for all compounds were collected at four different temperatures (100, 150, 200, and 295 K) on a Nonius KappaCCD diffractometer with graphite-monochromated Mo Kα radiation (λ = 0.71069 Å) equipped with a Cryostream 600 (Oxford Cryosystems) open-flow gas cryostat. No absorption and extinction corrections were applied. Data sets were integrated with the DENZO−SMN package.[25a] Structures were solved by direct methods with SIR97[25b] and refined (SHELXL97)[25c] by full-matrix least squares with anisotropic non-H and isotropic H atoms. All other calculations were accomplished using PARST[25d] and PLATON[25e] as implemented in the WINGX[25f] program system. The difference Fourier map of compound **1** shows a single maximum at bonding distance from the N atom, indicating the absence of proton disorder, while the Fourier maps of compounds **2** and **3** show, at all temperatures, diffuse electron densities between the N and O atoms with two maxima from which two proton positions can be identified. Refinement of the two H atoms with partial occupancies and isotropic thermal parameters fixed at 1.2 times those of the corresponding N or O atoms was successfully attempted, giving the final occupancy factors reported for both crystals at 100 K in Table 1 and for all temperatures in Table S1 (Supporting Information). Final Fourier difference maps at 100 K reported in Figures 1−3 have been obtained after least-squares refinement carried out starting from the final parameters but without the H-bond proton.

Crystal Data for 1 (100 K): $C_{17}H_{14}N_2O_2$, M_r = 278.30, monoclinic $P2_1/c$ (No. 14), a = 15.5544(4) Å, b = 5.5221(1) Å, c = 16.3325(5) Å, β = 108.268(1)°, V = 1332.14(6) Å^3, Z = 4, D_{calc} = 1.388 g cm^{-3}, μ = 0.93 cm^{-1}, and T = 100 K. A total of 3882 unique measured reflections ($\theta \le 30°$) were used in the refinement, out of which 2613 with $I \ge 2\sigma(I)$ were considered observed. R (on F^2, observed reflections) = 0.048, R_w (all reflections) = 0.141, and S = 1.06.

Crystal Data for 1 (150 K): $C_{17}H_{14}N_2O_2$, M_r = 278.30, monoclinic $P2_1/c$ (No. 14), a = 15.5766(3) Å, b = 5.5382(1) Å, c = 16.3781(5) Å, β = 108.061(1)°, V = 1343.26(5) Å^3, Z = 4, D_{calc} = 1.376 g cm^{-3}, μ = 0.92 cm^{-1}, and T = 150 K. A total of 3914 unique measured reflections ($\theta \le 30°$) were used in the refinement, out of which 2706 with $I \ge 2\sigma(I)$ were considered observed. R (on F^2, observed reflections) = 0.048, R_w (all reflections) = 0.140, and S = 1.05.

Crystal Data for 1 (200 K): $C_{17}H_{14}N_2O_2$, M_r = 278.30, monoclinic $P2_1/c$ (No. 14), a = 15.5907(3) Å, b = 5.5530(1) Å, c = 16.4284(4) Å, β = 107.792(1)°, V = 1354.27(5) Å^3, Z = 4, D_{calc} = 1.365 g cm^{-3}, μ = 0.91 cm^{-1}, and T = 200 K. A total of 3936 unique measured reflections ($\theta \le 30°$) were used in the refinement, out of which 2613 with $I \ge 2\sigma(I)$ were considered observed. R (on F^2, observed reflections) = 0.048, R_w (all reflections) = 0.142, and S = 1.04.

Crystal Data for 1 (295 K): $C_{17}H_{14}N_2O_2$, M_r = 278.30, monoclinic $P2_1/c$ (No. 14), a = 15.6361(3) Å, b = 5.5774(1) Å, c = 16.5550(5) Å, β = 107.267(1)°, V = 1378.67(6) Å^3, Z = 4, D_{calc} = 1.341 g cm^{-3}, μ = 0.89 cm^{-1}, and T = 295 K. A total of 3306 unique measured reflections ($\theta \le 28°$) were used in the refinement, out of which 2613 with $I \ge 2\sigma(I)$ were considered observed. R (on F^2, observed reflections) = 0.051, R_w (all reflections) = 0.144, and S = 1.15.

Crystal Data for 2 (100 K): $C_{16}H_{11}ClN_2O$, M_r = 282.72, monoclinic $P2_1/n$ (No. 14), a = 12.9391(3) Å, b = 3.8207(1) Å, c = 25.7129(6) Å, β = 91.617(1)°, V = 1270.65(5) Å^3, Z = 4, D_{calc} = 1.48 g cm^{-3}, μ = 2.96 cm^{-1}, and T = 100 K. A total of 3035 unique measured reflections ($\theta \le 28°$) were used in the refinement, out of which 2337 with $I \ge 2\sigma(I)$ were considered observed. R (on F^2, observed reflections) = 0.039, R_w (all reflections) = 0.105, and S = 1.09.

Crystal Data for 2 (150 K): $C_{16}H_{11}ClN_2O$, M_r = 282.72, monoclinic $P2_1/n$ (No. 14), a = 12.9526(3) Å, b = 3.8409(1) Å, c = 25.7179(7) Å, β = 91.557(1)°, V = 1278.98(6) Å^3, Z = 4, D_{calc} = 1.47 g cm^{-3}, μ = 2.94 cm^{-1}, and T = 150 K. A total of 3056 unique measured reflections ($\theta \le 28°$) were used in the refinement, out of which 2164 with $I \ge 2\sigma(I)$ were considered observed. R (on F^2, observed reflections) = 0.042, R_w (all reflections) = 0.111, and S = 1.09.

Crystal Data for 2 (200 K): $C_{16}H_{11}ClN_2O$, M_r = 282.72, monoclinic $P2_1/n$ (No. 14), a = 12.9684(3) Å, b = 3.8649(1) Å, c = 25.7294(7) Å, β = 91.476(1)°, V = 1289.17(6) Å^3, Z = 4, D_{calc} = 1.46 g cm^{-3}, μ = 2.92 cm^{-1}, and T = 200 K. A total of 3087 unique measured reflections ($\theta \le 28°$) were used in the refinement, out of which 2070 with $I \ge 2\sigma(I)$ were considered observed. R (on F^2, observed reflections) = 0.043, R_w (all reflections) = 0.113, and S = 1.13.

Crystal Data for 2 (295 K): $C_{16}H_{11}ClN_2O$, M_r = 282.72, monoclinic $P2_1/n$ (No. 14), a = 12.9932(5) Å, b = 3.9181(1) Å, c = 25.7473(9) Å, β = 91.307(2)°, V = 1310.42(8) Å^3, Z = 4, D_{calc} = 1.43 g cm^{-3}, μ = 2.87 cm^{-1}, and T = 295 K. A total of 3132 unique measured reflections ($\theta \le 28°$) were used in the refinement, out of which 2356 with $I \ge 2\sigma(I)$ were considered observed. R (on F^2, observed reflections) = 0.044, R_w (all reflections) = 0.121, and S = 1.08.

Crystal Data for 3 (100 K): $C_{18}H_{17}N_3O$, M_r = 291.35, monoclinic $P2_1/n$ (No. 14), a = 7.6125(1) Å, b = 7.9679(1) Å, c = 24.2654(5) Å, β = 98.660(1)°, V = 1455.05(4) Å^3, Z = 4, D_{calc} = 1.33 g cm^{-3}, μ = 0.85 cm^{-1}, and T = 100 K. A total of 4244 unique measured reflections ($\theta \le 30°$) were used in the refinement, out of which 3091 with $I \ge 2\sigma(I)$ were considered observed. R (on F^2, observed reflections) = 0.046, R_w (all reflections) = 0.136, and S = 1.06.

Crystal Data for 3 (150 K): $C_{18}H_{17}N_3O$, M_r = 291.35, monoclinic $P2_1/n$ (No. 14), a = 7.6179(3) Å, b = 7.9882(1) Å, c = 24.3423(6) Å, β = 98.648(1)°, V = 1464.47(4) Å^3, Z = 4, D_{calc} = 1.32 g cm^{-3}, μ = 0.84 cm^{-1}, and T = 150 K. A total of 3535 unique measured reflections ($\theta \le 28°$) were used in the refinement, out of which 2473 with $I \ge 2\sigma(I)$ were considered observed. R (on F^2, observed reflections) = 0.045, R_w (all reflections) = 0.131, and S = 1.07.

Crystal Data for 3 (200 K): $C_{18}H_{17}N_3O$, M_r = 291.35, monoclinic $P2_1/n$ (No. 14), a = 7.6238(1) Å, b = 8.0124(1) Å, c = 24.4421(5) Å, β = 98.641(1)°, V = 1476.10(4) Å^3, Z = 4, D_{calc} = 1.31 g cm^{-3}, μ = 0.84 cm^{-1}, and T = 200 K. A total of 3566 unique measured reflections ($\theta \le 28°$) were used in the refinement, out of which 2330 with $I \ge 2\sigma(I)$ were considered observed. R (on F^2, observed reflections) = 0.045, R_w (all reflections) = 0.133, and S = 1.10.

Crystal Data for 3 (295 K): $C_{18}H_{17}N_3O$, M_r = 291.35, monoclinic $P2_1/n$ (No. 14), a = 7.6328(1) Å, b = 8.0545(1) Å, c = 24.6916(6) Å, β = 98.640(1)°, V = 1500.77(5) Å^3, Z = 4, D_{calc} = 1.29 g cm^{-3}, μ = 0.82 cm^{-1}, and T = 295 K. A total of 3614 unique measured reflections ($\theta \le 28°$) were used in the refinement, out of which 1912 with $I \ge 2\sigma(I)$ were considered observed. R (on F^2, observed reflections) = 0.050, R_w (all reflections) = 0.159, and S = 1.10.

Acknowledgment. We thank CINECA, Casalecchio di Reno (Bologna), and INSTM (Florence) for free use of the IBM SP4

(25) (a) Otwinowski, Z.; Minor, W. In *Macromolecular Crystallography*; Carter, C. W., Jr. Sweets, R. M., Eds.; Methods in Enzymology 276; Academic Press: San Diego, CA, 1997; Part a, p 307. (b) Altomare, A.; Burla, M. C.; Camalli, M.; Cascarano, G. L.; Giacovazzo, C.; Guagliardi, A.; Moliterni, A. G.; Polidori, G.; Spagna, R. *J. Appl. Crystallogr*. **1999**, *32*, 115. (c) Sheldrick, G. M. *SHELXL97, Program for crystal structure refinement*; University of Göttingen: Göttingen, Germany, 1997. (d) Nardelli, M. *J. Appl. Crystallogr*. **1995**, *28*, 659. (e) Spek, A. L. *PLATON, A Multipurpose Crystallographic Tool*; Utrecht University: Utrecht, The Netherlands, 2002. (f) Farrugia, L. J. *J. Appl. Crystallogr*. **1999**, *32*, 837.

computer facility and MIUR (Rome) for COFIN 2004 financial support. L.A. thanks the A. von Humboldt Foundation for the Return Fellowship.

Supporting Information Available: Table S1, structural parameters for compounds **1**−**3** at all temperatures investigated; Table S2, additional geometrical information on DFT-emulated molecules; Table S3 and Figures S1 and S3, application of Marcus method to DFT-emulated molecules; Table S4, DFT geometries and energies; X-ray crystallographic files (12 CIF files). This material is available free of charge via the Internet at http://pubs.acs.org.

JA0453984